Hearing Research 440 (2023) 108911

Contents lists available at ScienceDirect

Hearing Research

journal homepage: www.elsevier.com/locate/heares

Spread of activation and interaction between channels with multi-channel optogenetic stimulation in the mouse cochlea

Ajmal A. Azees [a,b], Alex C. Thompson [a,f], Ross Thomas [a], Jenny Zhou [a], Patrick Ruther [c,d], Andrew K. Wise [a,e,f], Elise A. Ajay [a,g], David J. Garrett [b], Anita Quigley [b,h,i], James B. Fallon [a,e,f], Rachael T. Richardson [a,e,f,*]

[a] The Bionics Institute, East Melbourne, VIC 3002, Australia
[b] Department of Electrical and Biomedical Engineering, RMIT University, Melbourne, VIC 3000, Australia
[c] Department of Microsystems Engineering (IMTEK), University of Freiburg, Freiburg 79110, Germany
[d] BrainLinks-BrainTools Center, University of Freiburg, Freiburg 79110, Germany
[e] Department of Surgery (Otolaryngology), University of Melbourne, Melbourne, VIC 3002, Australia
[f] Medical Bionics Department, University of Melbourne, East Melbourne, VIC, Australia
[g] Faculty of Engineering and Information Technology, University of Melbourne, Melbourne, VIC, Australia
[h] Department of Medicine, University of Melbourne, St Vincent's Hospital, Melbourne, VIC 3065, Australia
[i] The Aikenhead Centre for Medical Discovery, St Vincent's Hospital, Melbourne, VIC 3065, Australia

ARTICLE INFO

Keywords:
Optogenetics
Cochlear implant
Channel interaction
Spread of activation
Electrical stimulation
Optical stimulation

ABSTRACT

For individuals with severe to profound hearing loss resulting from irreversibly damaged hair cells, cochlear implants can be used to restore hearing by delivering electrical stimulation directly to the spiral ganglion neurons. However, current spread lowers the spatial resolution of neural activation. Since light can be easily confined, optogenetics is a technique that has the potential to improve the precision of neural activation, whereby visible light is used to stimulate neurons that are modified with light-sensitive opsins. This study compares the spread of neural activity across the inferior colliculus of the auditory midbrain during electrical and optical stimulation in the cochlea of acutely deafened mice with opsin-modified spiral ganglion neurons (H134R variant of the channelrhodopsin-2). Monopolar electrical stimulation was delivered via each of four 0.2 mm wide platinum electrode rings at 0.6 mm centre-to-centre spacing, whereas 453 nm wavelength light was delivered via each of five 0.22 × 0.27 mm micro-light emitting diodes (LEDs) at 0.52 mm centre-to-centre spacing. Channel interactions were also quantified by threshold changes during simultaneous stimulation by pairs of electrodes or micro-LEDs at different distances between the electrodes (0.6, 1.2 and 1.8 mm) or micro-LEDs (0.52, 1.04, 1.56 and 2.08 mm). The spread of activation resulting from single channel optical stimulation was approximately half that of monopolar electrical stimulation as measured at two levels of discrimination above threshold ($p<0.001$), whereas there was no significant difference between optical stimulation in opsin-modified deafened mice and pure tone acoustic stimulation in normal-hearing mice. During simultaneous micro-LED stimulation, there were minimal channel interactions for all micro-LED spacings tested. For neighbouring micro-LEDs/electrodes, the relative influence on threshold was 13-fold less for optical stimulation compared electrical stimulation ($p<0.05$). The outcomes of this study show that the higher spatial precision of optogenetic stimulation results in reduced channel interaction compared to electrical stimulation, which could increase the number of independent channels in a cochlear implant. Increased spatial resolution and the ability to activate more than one channel simultaneously could lead to better speech perception in cochlear implant recipients.

Abbreviations: AAV, adeno associated virus; ChR2, channelrhodopsin-2; CL, current level; IC, inferior colliculus; LED, light-emitting diode; MP, monopolar; NBN, narrowband noise; RIE, reactive ion etching; CI, cochlear implant; SGN, spiral ganglion neuron.

* Corresponding author at: The Bionics Institute, East Melbourne, VIC 3002, Australia.
E-mail address: rrichardson@bionicsinstitute.org (R.T. Richardson).

https://doi.org/10.1016/j.heares.2023.108911
Received 16 June 2023; Received in revised form 19 October 2023; Accepted 2 November 2023
Available online 4 November 2023

1. Introduction

The cochlea of the inner ear is a specialised structure that separates acoustic vibrations into a tonotopic frequency map. Hair cells and spiral ganglion neurons (SGNs) are arranged along this map with the role of transducing sound information to the brain, but are susceptible to irreparable damage by noise exposure, infection, ototoxic drugs, age-related degeneration, or genetic defects. The resulting loss of sensitivity to sound is termed sensorineural hearing loss, affecting millions of people worldwide. People with severe or profound hearing loss receive significant utility from a cochlear implant (Wilson and Dorman 2008), an array of up to 22 electrodes that bypasses hair cells and electrically activates the residual SGNs. The cochlear implant is programmed to process sound into discrete frequency bands and delivers charge-balanced biphasic electrical pulses to specific electrodes according to the tonotopic frequency map. In theory, each electrode should excite a well-defined neural population and provide an independent channel of information, but in practice, neural excitation is spatially very broad, and the areas of activation overlap due to the conductive environment in the cochlea (Black et al. 1981, Snyder et al. 2004, George et al. 2014, George et al. 2015b). This spectral smearing is a main cause of poor pitch perception in cochlear implant recipients (Fu and Nogaki 2005), low speech intelligibility in the presence of background noise (Friesen et al. 2001), and poor speech intelligibility even in quiet environments for pitch-accent languages such as Persian (Poursoroush et al. 2015) or tonal languages like Mandarin (Huang et al. 2005).

Due to the issue of current spread, cochlear implant electrodes must be stimulated sequentially rather than simultaneously to avoid interactions between channel interactions which would otherwise lead to uncontrolled loudness and distortion of the signal. It is postulated that more focused stimulation would enable simultaneous stimulation of electrodes which could improve the spectral and temporal representation of sound and improve speech intelligibility and pitch perception (Friesen et al. 2001). Various electrode configurations have been proposed to deliver focused stimulation compared to monopolar (MP) configurations: bipolar, tripolar, focussed multipolar, and common ground. Previous studies using computational models showed that the tripolar configuration could deliver more focused stimuli and create more spatially focused electric fields than the MP or bipolar configurations (Litvak et al. 2007, Frijns et al. 2011, Kalkman et al. 2015). It has been confirmed in animal studies that current focusing configurations such as bipolar (Rebscher et al. 2001), tripolar (Snyder et al. 2004), focussed multipolar (George et al. 2015a) and partial tripolar (Landsberger and Srinivasan 2009) activate more restricted areas of the cochlea when compared to the MP configuration in the cochlear implant. Furthermore, channel interactions during focused multipolar stimulation and tripolar stimulation were significantly lower than during MP stimulation in the cat (George et al. 2015a). Despite the advantages shown in the animal studies using current focusing methods, MP stimulation is the widely used configuration in commercialised cochlear implants due to several factors, such as the higher power required for the current focussing method compared to MP stimulation (Pfingst and Xu 2004) and the inability to do multi-channel simultaneous stimulation to deliver fine temporal information. Hence, clinical studies suggest that current focusing techniques do not deliver any clinical benefit (Berenstein et al. 2008, Bierer and Litvak 2016).

Optical stimulation is an alternative technology that is widely used for neural modulation research and in development as a clinical neural modulation method. Infrared light has been shown to initiate action potentials in multiple neural systems (Wells et al. 2005, Peterson and Tyler 2013, Thompson et al. 2014, Cayce et al. 2014, Chernov and Roe 2014), and in the cochlea the area of excitation has been shown to be more spatially precise compared to electrical stimulation (Richter et al. 2011, Thompson et al. 2014, Agarwal et al. 2021). However, concerns over the mechanism of activation, potential for thermal damage, and high-power requirements has led to the study of other mechanisms of light-mediated activation. Recent development in optogenetics, in which visible light is used to activate neurons modified with light sensitive molecules called opsins (Deisseroth 2015), show that visible light can activate SGNs (Hernandez et al. 2014, Keppeler et al. 2018, Wrobel et al. 2018, Dieter et al. 2019, Keppeler et al. 2020, Thompson et al. 2020, Bali et al. 2021, Richardson et al. 2021, Bali et al. 2022) and deliver a spatially precise stimulus to the cochlea with much lower power (Dieter et al. 2019, Keppeler et al. 2020, Richardson et al. 2020, Thompson et al. 2020). Furthermore, high temporal precision can be obtained by combining optical stimulation with low level electrical stimulation, while retaining the spatial advantages of optical stimulation due to the lowering of the electrical threshold for stimulation (Thompson et al. 2020, Ajay et al. 2023). It has not yet been shown whether the higher spatial precision delivered by optical stimulation reduces channel interactions, essential for the development of simultaneous stimulation strategies which could increase speech intelligibility in cochlear implant recipients.

The primary objective of the study was to compare the degree of interaction between channels during optical stimulation, with comparisons to electrical stimulation or acoustic stimulation of the cochlea. Using mice that expressed the ChR2-H134R opsin in SGNs, spiking activity was measured in the inferior colliculus of the auditory midbrain during single-channel and multi-channel optical or electrical stimulation as a measure of the level and extent of cochlear activation. Optical or electrical stimulation were delivered separately to the cochlea via an array of 5 micro-LED-based optrodes (453 nm) or 4 platinum electrodes, respectively. Results were compared to acoustic stimulation with pure tones and narrowband noise (NBN) of different octave widths. Spread of activation was significantly lower for optical stimulation compared to electrical stimulation ($p<0.001$, $n=6$) and was not significantly different to pure tone acoustic stimuli ($p=0.373$, $n=6$). During simultaneous MP electrical stimulation there was a high degree of interaction for adjacent electrodes with a pitch of 0.6 mm. Conversely, simultaneous stimulation of micro-LEDs with a pitch of 0.52 mm had significantly lower interaction compared to MP electrical stimulation ($p<0.05$, $n=5$). The reduced channel interaction observed with optical stimulation could increase the number of independent channels in cochlear implants, thus leading to better speech recognition and frequency discrimination in cochlear implant recipients.

2. Methods

2.1. Animals and ethical approvals

A transgenic mouse model was used in this study that had ChR2-H134R-EYFP expression in all SGNs of the cochlea. The transgenic mice were derived from a cross between the B6;129S-Gt(ROSA)26Sor$^{tm32(CAG-COP4*H134R/EYFP)Hze/J}$ strain (The Jackson Laboratory #012569, backcrossed onto a C57BL/6 background) and B6;129P2-Pvalb$^{tm1(cre)Arbr}$ (The Jackson Laboratory #008069) and thus carry one allele for ChR2-H134R-EYFP. The mice express ChR2-H134R in all spiral ganglion neurons, inner hair cells and outer hair cells (Thompson et al. 2020) and exhibit normal hearing thresholds (Ajay et al. 2023). This study used 13 male mice and 5 female mice. The use and care of the experimental animals in this study were approved by St Vincent's Hospital Animal Ethics Committee, Melbourne, Australia (#21-007) following the Guidelines to Promote the Wellbeing of Animals used for Scientific Purposes (2013), the National Health and Medical Research Council Code for Care and Use of Animals for Scientific Purposes (8th edition, 2013) and the Prevention of Cruelty to Animals Amendment Act (2015).

2.2. Stimulating arrays

Electrode arrays were designed and fabricated by Neo-Bionica,

Melbourne, Australia. They consisted of 4 platinum rings, each 0.2 mm in length and tapering in diameter from 0.27 mm at the base to 0.21 mm at the tip of the array. Inter-electrode spacing (centre-to-centre) was fixed to 0.6 mm. The electrodes were connected by individual, insulated platinum-iridium wires (Pt90/Ir10) with a diameter of 0.25 μm. Wires were helically coiled to reduce mechanical stress. The space inside and in between electrodes was filled with medical grade silicone MED-4880 (NuSil Technology, CA, USA) applied in a moulding process. This allowed a 0.16 mm long cylindrical tip to be implemented. Electrodes were named as E1 to E4, where E4 is the tip electrode of the array (Fig. 1A).

The micro-LED-based optrode arrays consisted of 5 micro-LED chips (CREE C460TR2227, CREE, Durham, USA), each with a 0.27 × 0.22 mm footprint at an inter-LED spacing (centre-to-centre) of 0.52 mm. The micro-LEDs were assembled on a 10-μm-thick polyimide substrate (Ayub et al. 2017, Keppeler et al. 2020). This substrate was realized by spin-coating first a 5-μm-thin polyimide layer on a silicon wafer (diameter 100 mm), followed by the deposition and patterning of interconnecting metal tracks using sputter deposition of a metallic thin film and lift-off technology, respectively. The track thickness was increased by electroplating 1 μm of gold in order the reduce the electrical line resistance. This was followed by the deposition of a second polyimide layer to insulate the metal tracks. By applying reactive ion etching (RIE) using oxygen plasma, small openings were introduced into the top polyimide layer to access the metal tracks. A second metallization and electroplating step was used to define so-called bonding pads for the micro-LED chips and contact pads to a zero-insertion-force connector. Finally, the shape of the polyimide substrate was defined by a second RIE process step which trenched the stack of polyimide layers down to the silicon substrate. Prior to micro-LED assembly the substrates were peeled from the silicon wafer using tweezers. The micro-LED chips were assembled on the pads of the polyimide substrate by flip-chip bonding (Ayub et al. 2017, Keppeler et al. 2020). They were subsequently underfilled with a biocompatible adhesive (EPO-TEK 301-2, Epoxy Technology, Inc., Billerica, USA) to electrically insulate the contact pads located at the interface between micro-LED chips and polyimide substrate. By manually applying a fluoropolymer (CYTOP, Asahi Glass Co. Ltd., Tokyo, Japan) cured at 80°C, the assembled optrodes received a first encapsulation layer. A second, parylene-based encapsulation of the optrodes was deposited using the following process sequence: (i) cleaning of optrodes in isopropanol and soft baking at 80°C for 1 h, (ii) surface treatment with oxygen plasma applied for 2 min to enhance adhesion properties between CYTOP and parylene, and (iii) conformal coating of the polyimide substrate and micro-LEDs by a 5-μm-thick double layer of parylene using vapor deposition polymerization. Subsequently, a silicone mould coating was applied to enhance the optrode stiffness. The micro-LEDs of the optrodes were labelled L1-L5, with L5 being the tip LED (Fig. 1B, C).

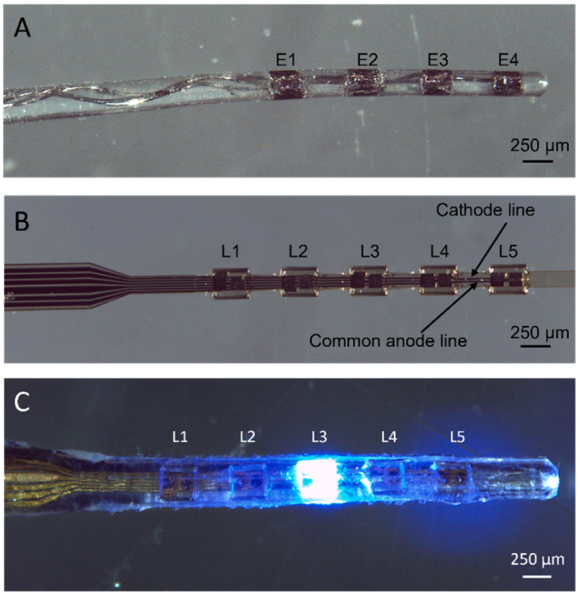

Fig. 1. Mouse multi-channel cochlear stimulating arrays
(A) Silicone-coated electrical array with 4 platinum ring-based electrodes 0.2 mm in length and tapering in diameter from 0.27 mm at the base electrode (E1) to 0.21 mm at the tip electrode (E4). Inter-electrode spacing is 0.6 mm. (B) Optrode array, consisting of a 10-μm-thin polyimide substrate with 5 micro-LEDs (0.27 × 0.22 mm; L1-L5) integrated at a pitch of 0.52 mm. The gold conducting lines tapered from 30 μm between the connector (towards the left, not shown) and micro-LEDs down to 5 μm in between the micro-LEDs. The optical array is shown here prior to encapsulation with parylene and silicone. (C) Mouse optical cochlear array, coated with parylene and silicone mould coating, with central micro-LED L3 switched on.

2.3. Anaesthesia, analgesia, and monitoring

At ~7-11 weeks of age, ChR2-H134R-EYFP transgenic mice were placed under gaseous anaesthesia (Isoflurane) to record multi-unit activity from the inferior colliculus in response to electrical or optical stimuli. Body temperature was maintained at 37°C with a heating pad and respiration was monitored throughout. Local anaesthesia (1 % lignocaine hydrochloride, *s.c.*) was applied to the wound margins of the cochlear and inferior colliculus surgical sites. Acoustic stimulation experiments, or experiments requiring the assessment of hearing, were performed under injectable anaesthesia (100 mg/kg ketamine mixed with 15 mg/kg xylazine, 0.1 mL/10 g, *i.p.*) due to isoflurane-mediated suppression of hearing thresholds and nerve fibre recruitment over time (Cederholm et al. 2012). Top-up doses were injected *s.c.* at 1/4 of the original dose every 30–45 min.

2.4. Surgical exposures

2.4.1. Cochlea

For electrical and optical stimulation experiments, the left cochlea was exposed to allow acute deafening and subsequent implantation of a multi-channel electrode array or a multi-channel optical array (see Section 2.5.1). A post-auricular incision was made, with the adipose and muscle layers gently separated to reveal the bulla. A #11 blade was used to hand-drill through the bulla. The bulla opening was expanded with angled forceps. The stapedial artery, which runs alongside the round window membrane, was cauterised with a bipolar electrocautery in some cases. In preparation for acute deafening, a cochleostomy was created in the apical region of the cochlea using a sharpened metal probe and the round window membrane was pierced with a pulled borosilicate pipette. Five microlitres of a 10 % (w/v) neomycin solution in saline was then applied slowly over 20 min to the round window membrane while gently aspirating using a suction pump from the apical cochleostomy site. This hair cell inactivation technique is known rapidly eliminate hair cell responses (Ajay et al. 2023). The surgical site was then temporarily plugged with a saline-soaked cotton ball during surgical exposure of the inferior colliculus. Surgical exposure of the cochlea was not required for acoustic stimulation experiments.

2.4.2. Inferior colliculus

Mice were placed in a stereotaxic frame (David Kopf Instruments) with the head secured via a bite-bar. A craniotomy was performed in the region of the intersection of the parietal and interparietal bones contralateral to the stimulated cochlea. The dura mater was gently removed to reveal the dorsal surface of the inferior colliculus.

2.5. Response data acquisition

2.5.1. Insertion of multi-channel stimulating arrays and multi-channel recording array

After the cochlear and inferior colliculus surgical sites were exposed, an electrode or optrode stimulating array was secured into an electrode holder and advanced gently via a micromanipulator into the cochlea until the final electrode or micro-LED was fully within the cochlea.

In order to measure multi-unit neural activity across the isofrequency laminae of the inferior colliculus (Landry et al. 2013, George et al. 2014, George et al. 2015b), a multi-channel recording array with 50 μm inter electrode spacing (NeuroNexus Technologies, MI, USA) was positioned vertically at the surface of the inferior colliculus 1 mm lateral to the lambda and slowly advanced (100 μm/s) along the dorsal-ventral axis of the inferior colliculus to a depth of approximately 1750 μm via a microdrive positioner (David Kopf Instruments, USA). During insertion, responses to the most apical electrodes/micro-LED were checked in the raster plot. Recordings were started approximately 5 min after electrode insertion, allowing time for the brain to settle and stabilise following the insertion process. Responses to acoustic, optical, or electrical stimuli recorded at the tip electrode were used to monitor the depth of insertion and ensure the recording array was within the central nucleus of the inferior colliculus. A 1 % (w/v) agar solution was applied to the surface of the inferior colliculus and around the recording array to provide stability to the recording array for neural recordings. The recording array was referenced via an internal reference that was kept in electrical contact with the brain via conductive agar and with grounding through a needle in the right axillary.

Stimulus waveforms were generated by an in-house purpose-built multi-channel stimulator controlled by custom software implemented in Igor Pro (Wavemetrics, Portland, OR). All combinations of stimuli were presented at random and repeated 10 times.

2.5.2. Acoustic stimuli

Open-field acoustic stimulation was delivered to normal hearing control mice only via a Tucker Davis Technologies SA1 Stereo Power Amp (TDT, USA) and a 4' Vifa XT25TG30-04 speaker (Speakerbits, Australia) at a rate of 4 Hz. The system was calibrated over a frequency range of 0.5–40 kHz. Acoustic stimuli were pure tone bursts or narrowband noise at 0.0625, 0.125, 0.25 and 0.5 octave widths (100 ms duration, 5 ms linear rise/fall), generated using custom designed software.

Frequency-place map for the mouse cochlea was expressed as with $F=3350(10^{0.0147x}-1)$, x in percentage distance from the apex (Ou et al. 2000b) and it was used to calculate the ocatve spacings of the electrodes/LEDs and the tone separations during simultaneous stimulation. An average length of 6.0 mm was assumed for C57BL/6 mice (Ou et al. 2000a, Keiler and Richter 2001, Keppeler et al. 2021).

Pure tone interference study: A pure tone input-output function was performed for six frequencies at 10-80 dB intensity range in 5 dB steps. Frequencies were based on the highest pure tone frequency (in the range of 36 kHz - 45 kHz) that could be reliably recorded in the inferior colliculus of each mouse (used as the interference channel; INT_{PT}) plus five test channel frequencies that were 0.25, 0.5, 1, 2 and 3 octaves below INT_{PT}. Having determined the threshold of INT_{PT}, the interference protocol was performed. INT_{PT} was fixed at one of four stimulus levels relative to its threshold (10 dB below threshold, at threshold, 10 dB above threshold and 20 dB above threshold, similar to those used in George et al. (2015a). The second simultaneous tone ($TEST_{PT}$) varied in frequency and stimulus intensity (10-80 dB SPL in 5 dB steps). Each combination of frequency and stimulus intensity of tones were presented in a random order with 10 repetitions.

Narrowband noise interference study: An input-output function was performed for narrowband noise at 0.0625, 0.125, 0.25 and 0.5 octave widths. The frequency of the interference channel narrowband noise was centred around the highest frequency that could be reliably recorded in the inferior colliculus of that mouse (INT_{NB}) and a second frequency (TEST) that was 0.25, 0.5, 1, 2 and 3 octaves below INT_{NB}. Intensities ranged from 10-80 dB and were presented in 5 dB steps, from which the INT_{NB} threshold was obtained. An interference protocol was run as per the pure tone study, with INT_{NB} fixed at one of four intensities and the simultaneous narrowband noise $TEST_{NB}$ presented at a range of intensities (10-80 dB SPL in 10 dB steps). This protocol was repeated for noise widths of 0.0625, 0.125 and 0.25 octaves.

2.5.3. Electrical stimuli

Biphasic, cathodic-first, charge-balanced electrical pulses were delivered via the platinum electrodes. For monopolar (MP) electrical stimulation (25 μs/phase with 8 μs interphase gap), an extracochlear stainless-steel needle placed subcutaneously in the left side axillary region of the mouse served as the return electrode. The amplitude of the electrical current was delivered in Current Levels (CL), where current in μA is given by: $I = 17.5 \times 100^{\frac{CL}{255}}$.

Electrical interference study: To generate MP electrical input-output functions, stimuli were delivered at 4 Hz over a range of current levels presented in 10 CL steps below myogenic threshold, each with 10 repetitions and presented in randomised order. The threshold of the most basal electrode (E1) was identified and used as the interference channel. The E1 interference channel (INT) was fixed at four stimulus levels (10 CL below threshold, at threshold, 10 CL above threshold and 20 CL above threshold, with the 10 CL steps chosen to be approximately 10 % above or below the threshold current level). Simultaneously, one of the other more apical (TEST) electrodes (E2-E4) was stimulated at a range of intensities in 10 CL steps.

2.5.4. Optical stimuli

Optrodes were operated by an in-house custom-designed LED driver and controlled by Igor Pro software (Wavemetrics, Portland, OR). Light was presented as 1-ms-long pulses at 4 Hz repetition rate. Currents between 0 and 10 mA were delivered, corresponding to an optical power of up to 3.4 mW linearly increasing with the micro-LED current (Ayub et al. 2017). The power output of micro-LED was measured with a power meter (LP10, Sanwa). At the given micro-LED currents, pulse duration and repetition rate, thermal effects due to tissue heating are expected to be negligible (Zgierski-Johnston et al. 2020).

Optical interference study: Optical stimuli were given at a rate of 4 Hz over a range of intensities up to 10 mA (3.4 mW) increased in steps of 0.2 mA (68 μW) to generate input output functions. The threshold of the most basal micro-LED L1 was identified and used as the interference channel. The L1 interference channel (INT) was fixed at four stimulus levels (0.2 mA below threshold, at threshold, 0.2 mA above threshold and 0.3 mA above threshold, with these values chosen to be approximately 10 % above or below the threshold stimulating intensity level. Simultaneously, one of the other more apical (TEST) micro-LEDs L2-L5 was stimulated at a range of intensities in 0.5 mA steps (170 μW).

2.6. Response data analysis

Multi-unit spike activity from each recording site was amplified, filtered, and digitised at a sample rate of 30 kHz using a Cerebus data acquisition system (Blackrock Microsystems, USA). Multi-unit activity was processed using customised spike detection scripts in Igor Pro (Wavemetrics, Portland, OR) as per previous studies (Thompson et al. 2020, Richardson et al. 2021). Spikes were detected at a level of four times the root mean square for threshold crossings for each recording channel. Spike counts were obtained from a 5 - 40 ms post stimulus window and converted to neural response strength by normalising between spontaneous activity and maximum driven spike rate for each stimulus protocol. Neural response strength across the array was colour-coded to display response images, with the electrode number of the recording array on the x-axis and the stimulus intensity on the y-axis.

A spatial tuning curve was generated by determining the threshold for each condition, defined as the lowest stimulus intensity to elicit a normalised spike rate of 0.3 (Landry et al. 2013). The recording site with the lowest threshold was defined as the best recording site (Fig. 2A).

2.6.1. Spread of activation

The widths of the spatial tuning curves were measured at two supra-threshold levels (cumulative d'=1 and d'=2 above threshold) for comparison between modalities, where the discrimination index (d') was used to quantify the growth in neural response with increasing stimulus intensity at each recording site (George et al. 2014). At the best recording site, the value of d' was cumulated across increasing stimulus levels above the threshold (Fig. 2A).

2.6.2. Channel interaction and threshold shift

Spiking activity at the best recording site was analysed to compare the interference between channels during simultaneous stimulation. Input-output curves were plotted from the spiking activity at each intensity, current level, or current value at the best recording site. Spiking activity was plotted for single channel stimulation (TEST) and simultaneous stimulation in the presence of an interference channel (INT) at four set levels relative to the threshold (sub threshold, at threshold and two supra-threshold levels).

The threshold shift difference at the best recording electrode during TEST channel stimulation was determined by Eq. (1) from the input-output curves.

$$\text{Threshold shift} = T_{INT+TEST} - T_{TEST} \quad \text{(Eq. 1)}$$

Where, $T_{INT+TEST}$ is the threshold of the best recording site of the test channel (F2-F5, E2-E4 or L2-L5) when stimulated simultaneously with an interference channel (F1, E1 or L1) and T_{TEST} is the threshold of test channel when it is stimulated alone. The threshold shift was measured in dB for sound, CL for electrical stimulation, and mW for light. A negative shift indicates the reduction of the threshold of the test channel when it is stimulated simultaneously with the interference channel, indicative of interaction between the two channels. When the spike rate did not cross 30 % of the maximum spiking activity, the threshold shift was determined by assigning the maximum stimulus level, for NBN 80 dB SPL and in the case of electrical, the threshold shift was assigned as 260 CL (Fig. 2B).

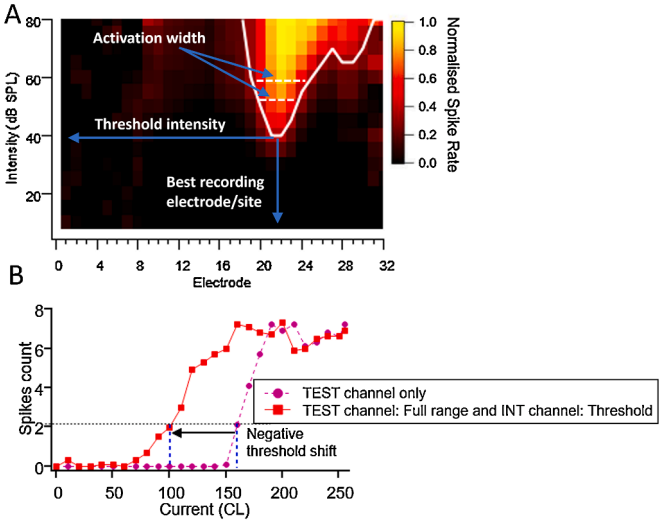

Fig. 2. Analysis of activation width, threshold, and threshold shift from IC response images (A) Response image generated based on the normalised spike rate at each stimulation intensity level, with zero corresponding to spontaneous activity (black) and one corresponding to maximum activity (yellow). The white line represents the spatial tuning curve, generated from the threshold (defined as 0.3 normalised spike rate) for each recording site. The best recording site was electrode 22 in this example with a threshold of 40 dB SPL. Activation width was measured at d'=1 and d'=2 above threshold (white dashed horizontal line). (B) Input-output curves based on the spike activity at each stimulus intensity level for the best recording site of test channel. The green dashed line indicates the spike rate when E2 is stimulated alone, and the red line indicates the spike rate when E1 is stimulated at a set intensity (in this case E1 is at threshold intensity) together with E2 at a range of intensities. A threshold shift in E2 resulting from interaction from E1 was calculated by subtracting the single-channel E2 threshold from the two-channel E2 threshold at the best recording site of E2 (-60 CL in this example) (n=1).

The relative influence of one channel on the other channel was quantitatively determined by dividing the reduction in the threshold by just noticeable difference (JND; Eq. (2)). JND was calculated by subtracting the threshold intensity from the intensity at which d'=1 when test channel was stimulated alone. Relative influence on threshold was averaged across all animals (n=5).

$$\text{Relative influence on the threshold} = \left\{\frac{Reduction\ in\ threshold}{JND}\right\} \quad \text{(Eq. 2)}$$

2.7. Statistical analysis

All data was tested for normality via the Shapiro-Wilk test. The Brown-Forsythe method was used to test equivalence of variance. Where the normality test failed, analysis of variation (ANOVA) on Ranks was performed. For the acoustic stimulation spread of activation data, a two-way analysis of variance (ANOVA) on Ranks (frequency x width of stimulus) was performed at two levels of discrimination above threshold (d'=1 and d'=2), followed by Holm-Sidak post-hoc analysis. To compare the spread of activation among electrical stimulation, optical stimulation, and acoustic (pure tone) stimulation, a two-way ANOVA on Ranks (stimulus type x channel; frequency/electrode/optrode) was performed for data measured at d'=1 above threshold, and a two-way ANOVA was performed on the data measured at d'=2 above threshold, each followed by Tukey post hoc analysis. A two-way ANOVA (width of stimulus x intensity of interference channel) was performed to identify the significance of threshold shift among different type of acoustic stimulation during the interference stimulation, followed by Tukey post hoc analysis. Two-way ANOVA on Ranks (stimulus type x intensity of interference channel) was performed to examine the significance of interactions between electrical, optical and acoustic stimulation with the relative influence on the threshold. A significance level of $p < 0.05$ was adopted as the criterion for statistical significance.

3. Results

3.1. Spread of activation

Inferior colliculus (IC) response images to acoustic stimuli were generated from normal hearing mice, for which the best recording site shifted towards the deeper recording sites (indicated by a higher electrode number) as the frequency was increased (Fig. 3). The spread of activation was measured at d'=1 above threshold for pure tone stimuli at five different frequencies (Fig. 3A), as well as narrowband noise (NBN) at four different stimulus widths (0.0625, 0.125, 0.25 and 0.5 with the same centre frequency as the pure tones; NBN 0.25 shown in Fig. 3B). The activation widths were compared by a two-way ANOVA on Ranks (frequency x stimulus width). There were significant main effects of stimulus widths ($f=10.868$, $p<0.001$), but not of frequencies ($f=2.411$, $p=0.053$). The same was found for the activation widths measured at d'=2. Therefore, the spread of activation was averaged across the different frequencies (9-36 kHz) for all the stimulus widths tested (Fig. 3C). The mean activation width for pure tone stimuli was 0.16 ± 0.03 mm when mesaured at d'=1 above threshold and 0.26 ± 0.04 mm when measured at d'=2 above threshold (n=6 mice). Activation widths at d'=1 above threshold for NBN 0.0625 (0.20 ± 0.03 mm)

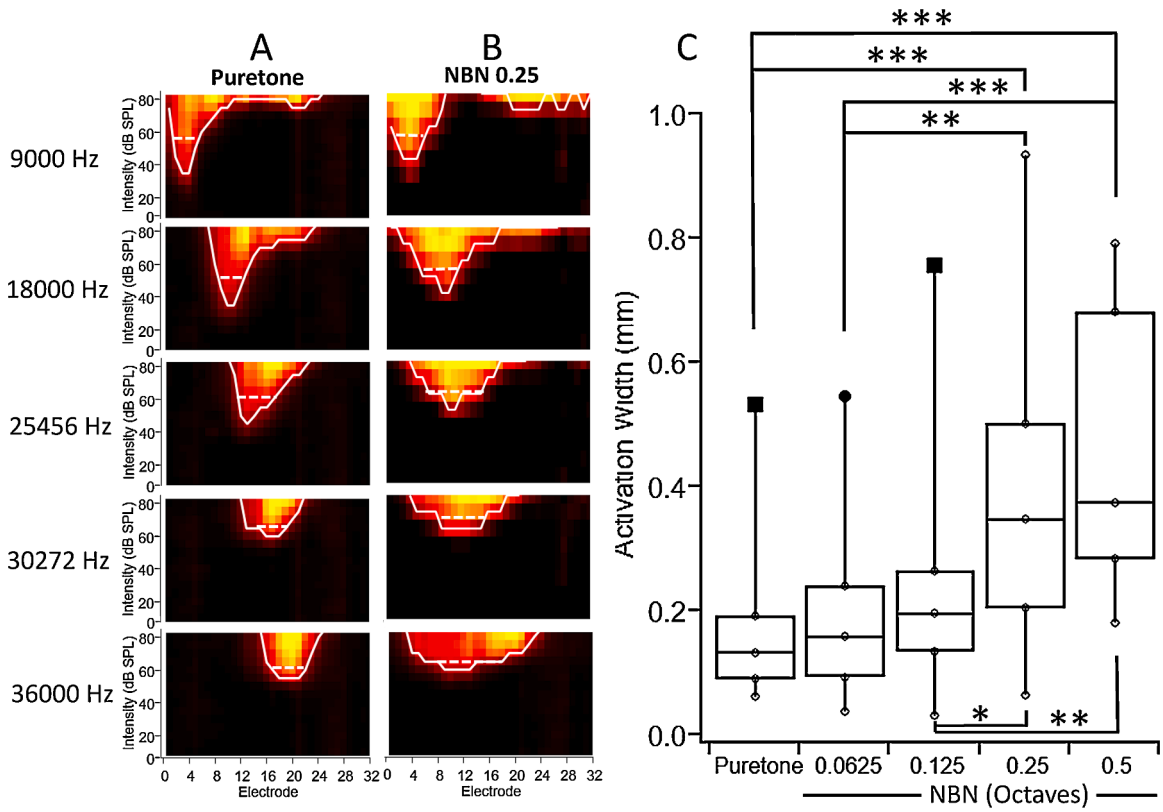

Fig. 3. Spatial extent of multi-unit activity across the recording sites in the IC to acoustic stimulation. (A) Representative response images to pure tone acoustic stimulation (9 - 36 kHz) in one mouse. (B) Narrowband noise stimulation with 0.25 octave width (centre frequency of 9 - 36 kHz), data from the same mouse as in A. The normalised spike rate at each stimulation intensity level is indicated by the colour scale as per Fig. 2A. The spatial tuning curve (solid white line) and the width of the spatial tuning curve at d'=1 above threshold (dashed white lines) are illustrated. (C) Box plot (medians and quartiles) representing activation width for acoustic stimulation with pure tones or narrowband noise at 4 different octave widths, measured at d'=1 above threshold and averaged across all frequencies (two-way ANOVA with Holm-Sidak post-hoc analysis, * p<0.05, ** p<0.01, ***p<0.001, n=6). Filled circle markers indicate outliers, filled square markers indicate far outliers (Tukey's method).

and for NBN 0.125 (0.24 ± 0.03 mm) were not significantly different to pure tone stimuli (Holm-Sidak post-hoc analysis, p=0.71 for NBN 0.0625 and p=0.24 for NBN 0.125, n=6, Fig. 3C). However, when the widths of the NBN were increased to 0.25 and 0.5 octaves, the spread of activation at d'=1 above threshold was significantly broader compared to pure tone, at 0.40 ± 0.03 mm and 0.42 ± 0.05 mm, respectively (n=6, p<0.001; Fig. 3C). Similar results were observed for spread of activation measured at d'=2 above threshold (n=6, Supplementary Fig. 1).

Acutely deafened mice were used for electrical and optical stimulation studies. Representative response images shown in Fig. 4 demonstrate the spatial extent of multi-unit activity in the IC to MP stimulation with E1 - E4, or optical stimulation with L1-L5. Similar to acoustic stimulation, the best recording site shifted towards the deeper sites when changing the electrodes/micro-LEDs from apical (E4 or L5) to basal (E1 or L1). During electrical stimulation, there was neural spiking activity across nearly all recording sites in the IC even when the stimulating currents were just 10-20 CL above the threshold (Fig. 4A). In contrast, spiking activity was more confined during optical stimulation, remaining so even as the stimulating intensity was increased (Fig. 4B).

The activation width across for electrical stimulation, optical stimulation, and pure tone acoustic stimulation were compared by a two-way ANOVA on Ranks (stimulus modality x channel) at discrimination levels of d'=1 and d'=2 above threshold. For activation widths measured at d'=1 above threshold, there were significant main effects of stimulus modalities (f=20.497, p<0.001), but not channels (f=0.611, p=0.066). The same was found for the activation widths measured at d'=2 above threshold (two-way ANOVA, f=29.12, p<0.001 for stimulus modality, and f=0.63, p=0.64 for channels). Therefore, the spread of activation was averaged across the different channels for the three stimuli tested. The spread of activation during optical stimulation (averaged across all micro-LEDs) measured at d'=1 and d'=2 above threshold was 0.22 ± 0.04 mm and 0.38 ± 0.04 mm, respectively (Fig. 5 A, B). Tukey post-hoc analysis revealed that the spread of activation for optical stimulation was significantly narrower than the spread of activation during MP electrical stimulation (averaged across all electrodes). At d'=1 and d'=2 above threshold, the spread of activation during the MP stimulation was approximately double that of optical stimulation, measuring 0.47 ± 0.04 mm and 0.74 ± 0.05 mm, respectively (Tukey post-hoc analysis p<0.001 for both d'=1 and d'=2, n=6; Fig. 5 A, B). Comparing to pure tone acoustic stimulation, the spread of activation during optical stimulation was not significantly different (p=0.37 for d'=1 and p=0.13 for d'=2, n=6, Fig. 5 A, B). The spread of activation during the electrical and optical stimulation is shown against pure tone and the four NBN octave widths for comparison purposes at d'=1 above threshold (Fig. 5C) and d'=2 above threshold (Fig. 5D). The spread of activation in the cochlea during optogenetic stimulation at d'=1 and d'=2 was similar to the spread observed during narrowband noise of 0.125 octaves. Conversely, the extent of activation during electrical stimulation was similar to that of the narrowband noise of 0.5 octaves (Fig. 5 C,D).

3.2. Channel interaction

Channel interactions were examined in response to two channel (TEST and INT) simultaneous acoustic stimulation in normal hearing

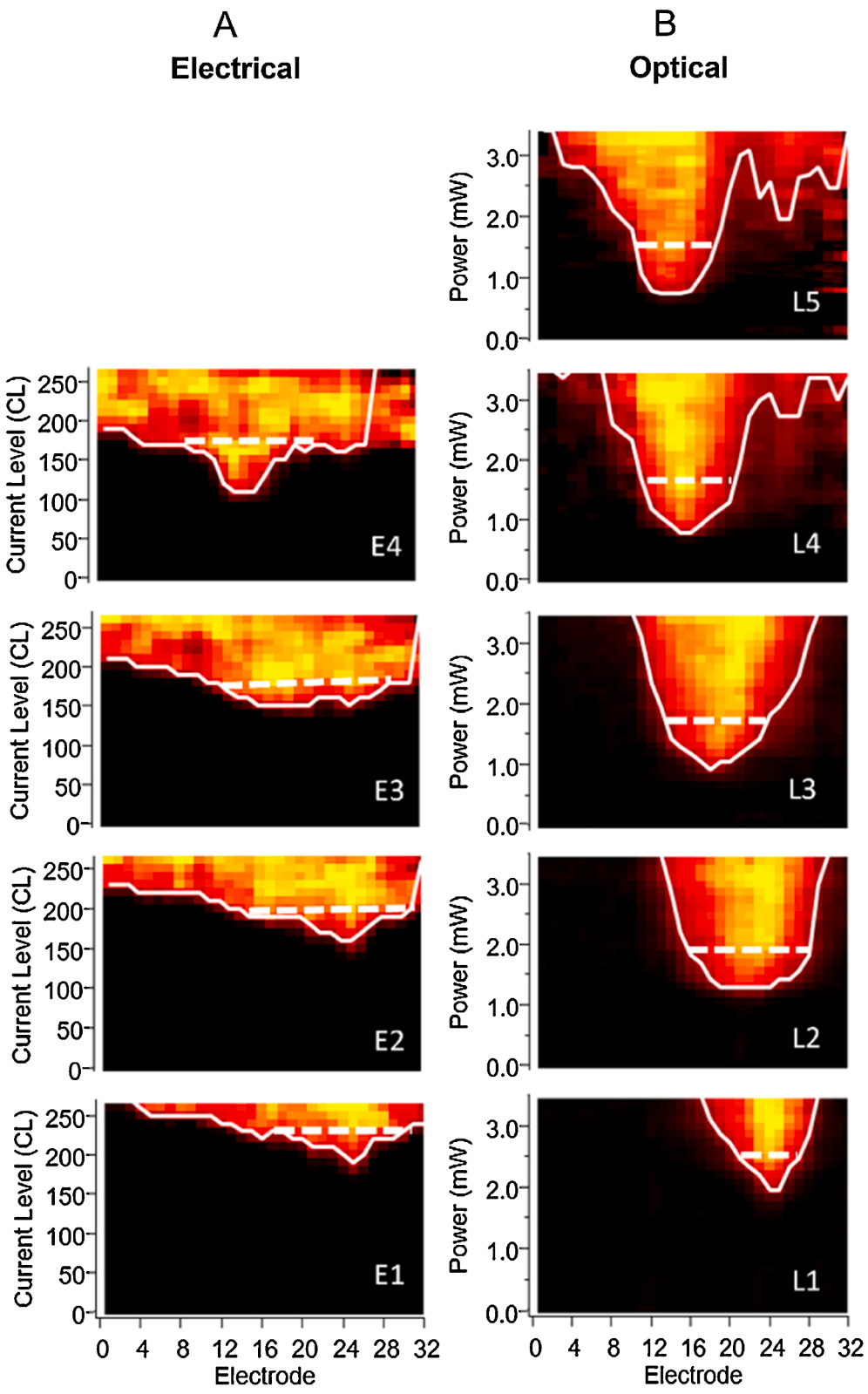

Fig. 4. Spatial extent of multi-unit activity across the recording sites in the IC to electrical and optical stimulation (A) Representative response images showing the spatial extent of multi-unit activity across the recording sites in the IC to monopolar electrical stimulation with each of the 4 electrodes (E1-E4) stimulated independently. (B) IC response images to optical stimulation with each of the 5 micro-LEDs stimulated independently (L1-L5; data from the same mouse as in A). The normalised spike rate at each stimulation intensity level is indicated by the colour scale as per Fig. 2A. The dotted white horizontal line in the response images indicates the activation width at d'=1 above threshold. L1 and E1 are closest to the base of the cochlea, positioned just inside the round window membrane.

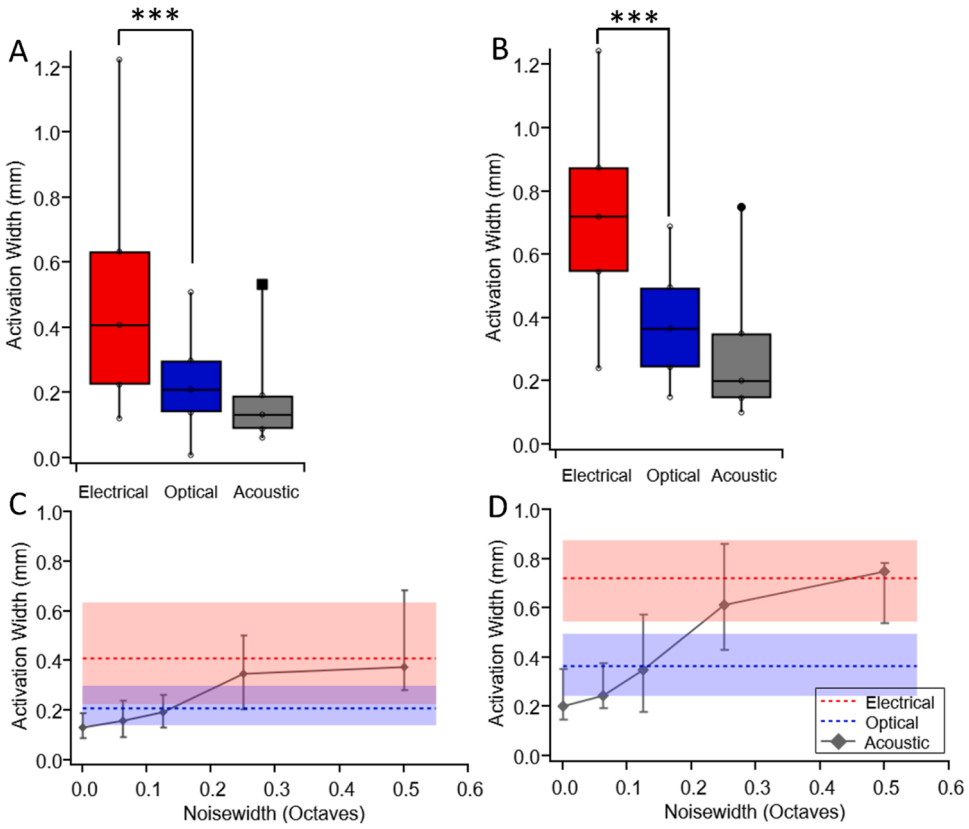

Fig. 5. Comparison of activation width for electrical, optical, and acoustic stimulation (A) Activation width for MP electrical, optical, or pure tone acoustic stimulation, measured at d'=1 above threshold and averaged across all stimulating electrodes, micro-LEDs, or frequencies (*** $p<0.001$, two-way ANOVA with Tukey post-hoc analysis, n=8 for electrical and n=6 for acoustic and optical). (B) Activation width for MP electrical, optical, or pure tone acoustic stimulation, measured at d'=2 above threshold and averaged across all stimulating electrodes, micro-LEDs, or frequencies (*** $p<0.001$, two-way ANOVA with Tukey post-hoc analysis, n=8 for electrical and n=6 for acoustic and optical). In A and B, filled circle markers indicate outliers, filled square markers indicate far outliers (Tukey's method). (C) Activation width at d'=1 above threshold during electrical stimulation (red) and optical stimulation (blue) in deafened mice (n=6-8), plotted alongside the activation width collected from normal hearing mice (n=6) during acoustic stimulation using pure tone and NBN (grey). (D) As per (C) at d'=2 above threshold. In C and D, dotted lines and data points represent the median values, and error bars and shading show the interquartile range.

mice and in response to two channel simultaneous optical and electrical stimulation in deafened mice.

For acoustic interaction studies, stimuli were presented at different pure tone frequency spacings (INT_{PT} and $TEST_{PT}$) and different narrowband noise with the same centre frequency spacings as the pure tones (INT_{NB} and $TEST_{NB}$). In the example in Fig. 6A where INT_{PT} was 36 kHz and $TEST_{PT}$ was 25 kHz (0.5 octave spacing), there was little impact on the threshold of the $TEST_{PT}$ best recording electrode at any of the INT_{PT} interference channel intensity levels, indicating that no interaction between the two tones occurred. Narrowband noise was then presented at three different noise widths 0.0625, 0.125 and 0.25. Response images with 0.125 and 0.25 octave width narrowband noise are shown in Fig. 6 B and C respectively. In all cases, interaction was evident between the INT_{NB} and $TEST_{NB}$, as indicated by a reduction in threshold for $TEST_{NB}$ when INT_{NB} was presented at 10 dB or more above threshold.

For simultaneous optical and electrical stimulation, different inter-channel spacings were used with reference to the most basal channel (E1 or L1). Examining adjacent channels first, the E1 or L1 interference channel was held at one of four constant sub- or supra-threshold current/power levels, while the test channel was presented at a range of intensities. The example in Fig. 6D shows adjacent electrodes E1 (INT channel) and E2 (TEST channel) with a centre-centre pitch of 0.6 mm (corresponding to ~0.5 of an octave gap) stimulated independently and simultaneously in the MP configuration. During simultaneous stimulation, the interaction between this electrode pair, as measured by the reduction in the threshold of E2 best recording electrode, occurred at all interference levels, even when E1 was stimulated at 10 CL below threshold. In contrast, for adjacent micro-LEDs L1 and L2 with a centre-to-centre pitch of 0.52 mm (corresponding to ~0.5 of an octave gap), there was minor interaction at the suprathreshold interference stimulation intensities (Fig. 6E).

Fig. 7 represents another set of response images generated during simultaneous stimulation at a greater distance between the TEST channel and INT channel. When there was one octave spacing between the interference and test frequencies (INT_{PT} was 36 kHz and $TEST_{PT}$ was 18 kHz respectively), there was no impact on the threshold of the test frequency best recording electrode at any of the interference frequency intensity levels, indicating that no interaction between the two tones occurred (Fig. 7A). Narrowband noise was then presented at three different noise widths 0.0625, 0.125 and 0.25. Response images with 0.125 and 0.25 octave width narrowband noise are shown in Fig. 7 B and C, respectively. In all cases, when INT_{NB} was presented at 10 dB or more above threshold, interaction was evident between the INT_{NB} and $TEST_{NB}$, as indicated by a reduction in threshold for $TEST_{NB}$.

Fig. 7D shows an example of single channel and simultaneous MP stimulation of electrode pairs E1 (INT channel) and E4 (TEST channel) with a centre-centre pitch of 1.8 mm. Despite the approximate one octave spacing of the electrodes, there was a reduction in threshold (from 110 CL to 80 CL) on the test channel indicating interaction between channels. In contrast, for micro-LEDs L1 (INT channel) and L4 (TEST channel) with a centre-to-centre pitch of 1.56 mm (corresponding to ~1 octave gap), there was no more than 0.12 μW shift at the suprathreshold interference stimulation intensities (Fig. 7E).

For each stimulation modality, plots of normalised spike rates versus

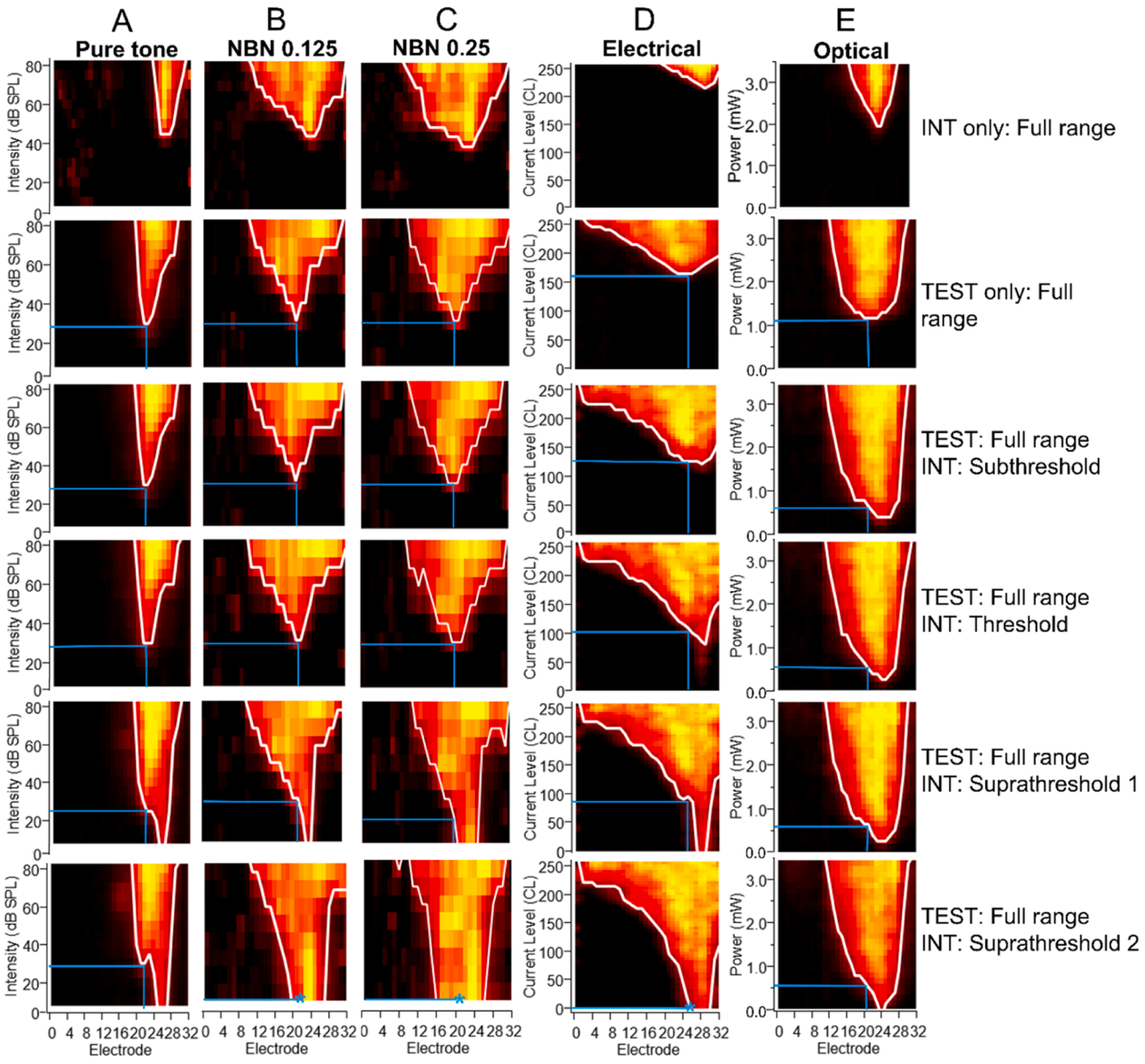

Fig. 6. IC response images generated during single channel and simultaneous stimulation with channels at minimum separation. For each stimulation mode, response images to single channel stimulation are shown in rows 1-2, and response images to simultaneous stimulation are shown in rows 3-6. During simultaneous stimulation, the interference channel (INT) was held at subthreshold (row 3), threshold (row 4), or two suprathreshold levels (rows 5-6), while the test channel (TEST) was presented at a range of intensities. The normalised spike rate at each stimulation intensity level is indicated by the colour scale as per Fig. 2A. (A) Pure tone acoustic stimulation in normal hearing mice, with INT at 36 kHz and TEST at 25 kHz (0.5-octave width below INT). (B) Narrowband noise stimulation at 0.125 octave width in normal hearing mice. Interference centre frequency 36 kHz, test centre frequency 25 kHz (C) Narrowband noise stimulation at 0.25 octave width in normal hearing mice. Interference center frequency 36 kHz, test center frequency 25 kHz. (D) MP electrical stimulation in deafened mice using neighbouring electrodes E1 (INT) and E2 (TEST) with a pitch of 0.6 mm. (E) Optical stimulation in deafened mice using neighbouring LEDs L1 and L2 with a pitch of 0.52 mm. (Blue vertical lines show the best recording electrode for TEST channel when stimulated independently. Blue horizontal lines show the threshold for the TEST channel when stimulated independently or simultaneously with the INT channel. Blue asterisks show the threshold of best recording site of TEST channel at zero intensity when it was stimulated with the INT channel at supra threshold 2. Suprathreshold 1 refers to the interference levels of threshold + 10 dB/CL and suprethreshold 2 refers to the interference level of threshold + 20 dB/CL.

stimulus intensity were generated for the best recording site of the test channel to compare threshold shifts for each inter-channel spacing or octave gap and each interference level. Acoustic octave gaps were 0.25, 0.5, 1.0 and 2.0. Electrode spacings were 0.6, 1.2 and 1.8 mm, and micro-LED spacings were 0.52, 1.04, 1.56 and 2.08 mm. For acoustic stimulation, regardless of the gap in the pure tone acoustic stimuli, there was very little apparent effect on the threshold of $TEST_{PT}$, except for minor interference when the intensity of INT_{PT} was 20 dB above the threshold (Fig. 8 A–D). In contrast, for each NBN width (0.0625, 0.125 and 0.25 octave widths), the threshold shift of $TEST_{NB}$ increased with increasing INT_{NB} interference intensity level, suggesting strong interaction between the acoustic stimuli. This interaction increased as the gap between the frequencies decreased. Furthermore, the broader NBN widths had a greater effect on the threshold shift at supra threshold intensity levels (two-way ANOVA with Tukey post-hoc analysis $p<0.05$) (Fig. 8 A–D).

For electrical stimulation, as the inter-electrode spacing decreased, there was an increase in the difference in threshold between single channel stimulation and simultaneous channel stimulation (threshold shift) for every level of interference (Fig. 8E-H). In contrast, for optical

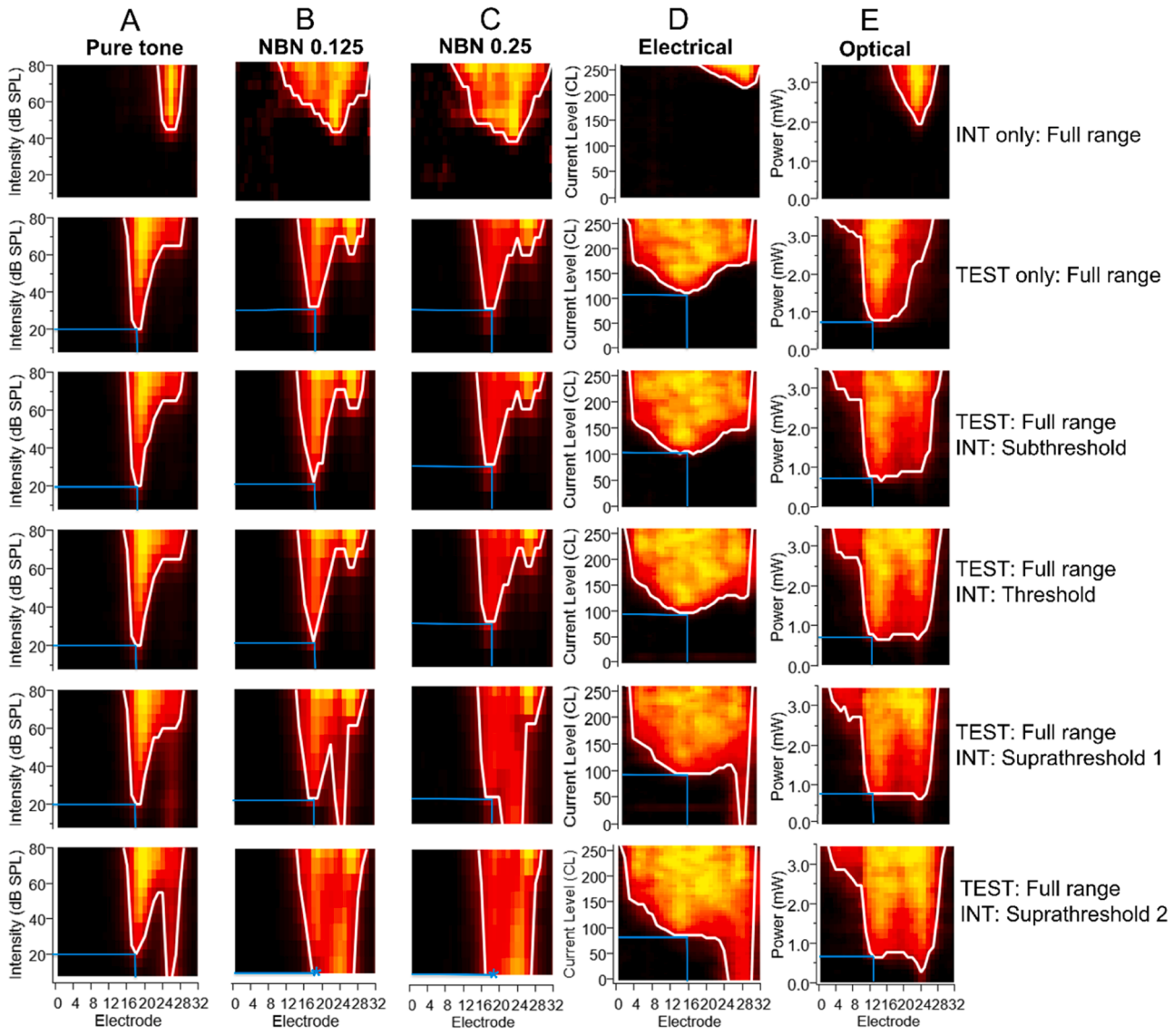

Fig. 7. IC response images generated during single channel and simultaneous stimulation with channels at maximum separation. Response images generated during single channel and simultaneous channel acoustic, electrical and optical stimulation with the same layout as Fig. 6 but with greater spacing between the channels. (A) Puretone acoustic stimulation, INT at 36 kHz and TEST at 18 kHz (1 octave width below INT). (B-C) Narrowband noise stimulation at 0.125 and 0.25 octave width. INT centre frequency was 36 kHz and TEST centre frequency was 18 kHz. (D) MP electrical stimulation using maximally distant electrodes E1 (INT) and E4 (TEST) with a pitch of 1.8 mm. (E) Optical stimulation using LEDs L1 (INT) and L4 (TEST) with a pitch of 1.56 mm. For further details, refer to Fig. 6.

stimulation there was minimal change in threshold at any inter-LED spacing or any interference level (Fig. 8E-H). Since the scale for electrical stimulation units is logarithmic and optical stimulation is measured on a linear scale, the relative influence on the threshold of the TEST channel during simultaneous stimulation on the INT channel is shown in Fig. 9. The relative threshold influence during electrical, optical and acoustic stimulation was calculated using Eq. (2) for paired channels when the INT channel was stimulated at subthreshold, threshold, or two suprathreshold intensity levels and the TEST channel was stimulated at a full range of intensities, and compared by a two-way ANOVA (stimulus type x interference channel intensity). There was a significant difference in the mean values of relative threshold influence ($f=16.76$, $p<0.001$), but not the interference channel intensity ($f=0.87$, $p=0.46$). For simultaneous electrical stimulation of neighbouring electrodes (0.6 mm pitch), the relative influence on threshold of the test channel was 19.69 when the neighbouring interference channel was at threshold (Fig. 9 B). For optical stimulation of neighbouring micro-LEDs (0.52 mm pitch), the relative influence on threshold was 1.46, which is 13.5 fold lower compared to electrical stimulation despite the lower pitch of the micro-LEDs ($p<0.05$, Tukey post-hoc analysis, $n=6$; Fig. 9 B). When the INT channel was at suprathreshold levels (1 and 2), the relative threshold influence reduced by 14-fold and 15-fold respectively ($p<0.05$ for suprathreshold 1 and $p<0.01$ for suprathreshold 2, Tukey post-hoc analysis, $n=6$), but the difference in relative threshold influence for subthreshold interference was not significant ($p=0.25$, Tukey post hoc analysis, $n=6$). The relative threshold influence was reduced when the distances between electrodes/micro-LEDs were increased.

4. Discussion

While the cochlear implant has up to 22 individual electrodes to deliver frequency information to the cochlea, the effective number of independent information channels is markedly lower due to the overlapping spread of excitation from the electrical current. As reported by Wolf et al. the necessity to enhance hearing restoration remains unaddressed with the present cochlear implant technologies (Wolf et al.

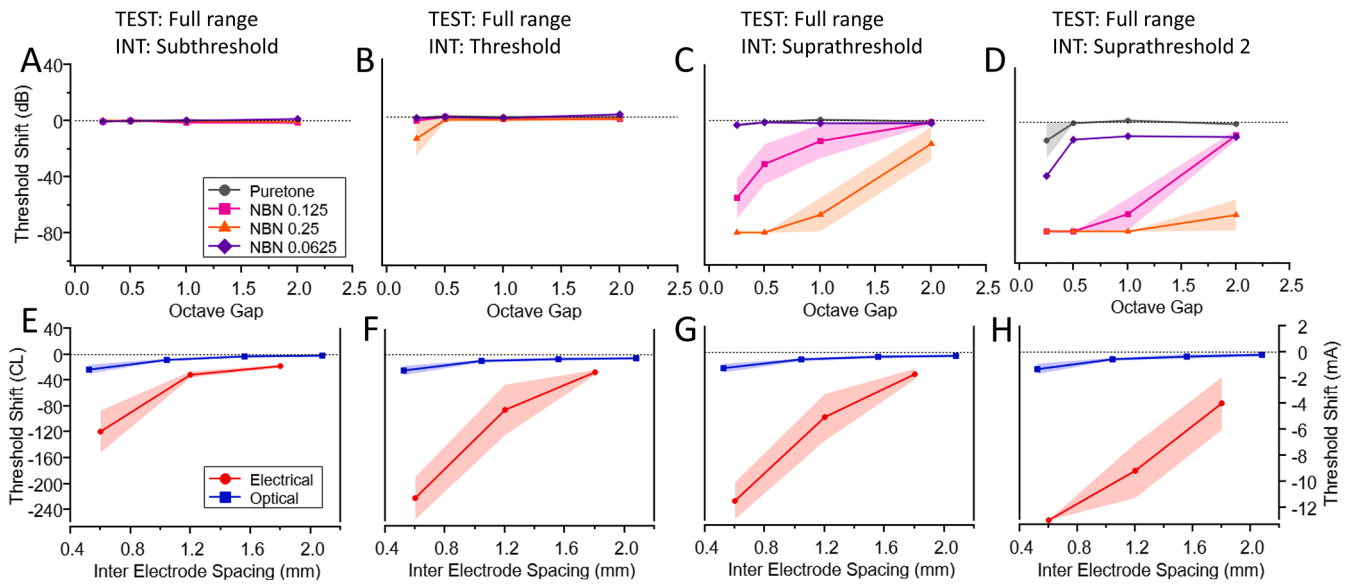

Fig. 8. Threshold shifts during simultaneous stimulation (A-D) Mean threshold shifts for the TEST channel at the best recording site for pairs of simultaneous tones or narrowband noise (NBN at 0.0625, 0.125 and 0.25 octave widths) presented at different octave gaps in normal hearing ChR2-H134R-EYFP transgenic mice. The INT channel was held at 4 intensities relative to threshold: (A) 10 dB below threshold, (B) at threshold, (C) 10 dB above threshold, and (D) 20 dB above threshold (n=6 mice). (E-H) Mean threshold shifts for the TEST channel at the best recording site for pairs of simultaneous electrodes or micro-LEDs presented at different spacing in deafened ChR2-H134R-EYFP transgenic mice. The E1 or L1 (INT) channel was held at one of four intensities relative to threshold: (E) 10 CL/0.2 mA below threshold (subthreshold), (F) at threshold, (G) 10 CL/0.2 mA above threshold and (H) 20 CL/0.3 mA above threshold (n=5 mice). For E-H, electrical stimulation threshold shift scale is shown on the left side Y axis and optical stimulation threshold shift is shown on the right side Y axis. For all graphs, the shaded regions show the standard error of the mean.

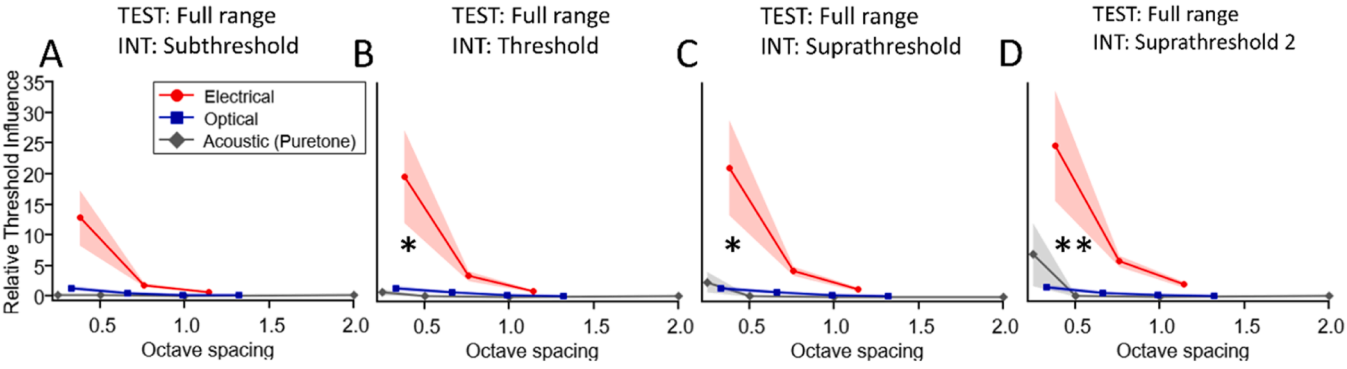

Fig. 9. Relative threshold influence during simultaneous stimulation (A-D) Relative influence on the threshold of the interference (INT) channel on the test (TEST) channel when it was stimulated simultaneously at different octave spacings. The TEST channel was presented at a range of intensities while the INT channel was held at (A) subthreshold, (B) threshold, (C-D) two levels above threshold for the electrical, optical and pure tone acoustic stimulation (n=5-6 mice). Asterisks denote statistical significance (two-way ANOVA with Tukey post-hoc analysis, *p<0.05, **p<0.01) for the comparison between electrical and optical stimulation for neighbouring electrodes. The shaded regions show the standard error of the mean.

2022). Optical stimulation has the potential to improve the precision of neural activation as light can be easily confined. The present study investigated the spread of activation and interactions between channels during stimulation with a multi-channel micro-LED optical array implanted in the cochlea of an optogenetic mouse model. To the best of our knowledge, this is the first study measuring the interaction between channels for optogenetic-based optical stimulation and the first to estimate the spread of optical and electrical stimulation via comparisons to acoustic narrowband noise. The results showed that the spread of activation during optical stimulation was significantly more restricted compared to electrical stimulation and was similar to pure tone acoustic stimulation, as measured at two levels of discrimination above threshold. Importantly, at high optical intensity levels, the IC response images remained narrow, whereas high electrical stimulation tended to result in activity across the entire recording array. Accordingly, the interaction between channels during optical stimulation was significantly lower compared to electrical stimulation. The improved spatial resolution of optical stimulation could be used to increase the number of independent channels and permit the use of simultaneous stimulation strategies.

4.1. *Optical stimulation in the cochlea*

One of the first demonstrations of how optical stimulation reduces the extent of cochlear activation was with infrared neural stimulation. Infrared radiation was directed towards the modiolus via an optical fibre 200 μm in diameter inserted into the acutely deafened guinea pig cochlea through a cochleostomy. Response curves with single or multiple peaks were observed with narrow spatial tuning curves that were similar to acoustic response curves (Richter et al. 2011). Infrared radiation has

the advantage of not requiring genetic modification of the SGNs. Conversely, optogenetic methods rely on the presence of opsins introduced to the neurons by viral vectors or transgenic mouse models. In Mongolian gerbils injected with adeno-associated virus (AAV) to transduce the SGNs with the Channelrhodopsin-2 variant CatCh, the auditory pathway was activated via visible light (473 nm), delivered to the cochlea with a 200 μm optical fibre inserted through the round window of the cochlea or via a cochleostomy in the middle and apex of the cochlea (Dieter et al. 2019). Again, the spatial tuning curves more closely resembled those of acoustic stimulation, whereas the extent of cochlear excitation for electrical stimulation was very broad (Dieter et al. 2019).

The method of delivering light to the SGNs has a big impact on spread of activation. When using an optical fibre inserted into the round window to deliver 488 nm laser light to ChR2-H134R transgenic mice (Thompson et al. 2020), the resulting area of activation was broader compared to the activation width achieved via implanted micro-LEDs presented in this study. While a laser-coupled optical fibre with a Gaussian emission profile should deliver more focussed light compared to the micro-LEDs used here characterized by a Lambertian emission profile, the angle of the optical fibre inserted into the round window of the cochlea is not optimal for SGN activation, and can result in activation of the central fibres of the SGNs (Dieter et al. 2019). However, when the optical fibre is inserted via a cochleostomy, the fibre is better angled towards the modiolus, resulting in more precise neural activation (Dieter et al. 2019, Richardson et al. 2021). Likewise, with an array of micro-LEDs as used in our study, the light is delivered towards the modiolus and the close proximity to the spiral ganglion means that there is limited loss of intensity or spread. Consequently, a more focussed optical stimulus is delivered to the SGNs despite the Lambertian emission profile of the micro-LEDs. Application of micro-lenses to micro-LED-based optrode arrays can potentially narrow the emission cone of the micro-LEDs further and increase the efficiency of light delivery to the SGNs (Klein et al. 2019). Using micro-LED-based optrodes similar to this study but realized using a different fabrication process (Klein et al. 2018), Dieter et al. investigated the activation of CatCh-transduced SGNs in Mongolian gerbils. Arrays consisted of 16 micro-LEDs with a footprint 60 × 60 μm and a pitch of 100, 150, or 250 μm. Blocks of 4 micro-LEDs were required to activate the SGNs, with the resulting spread of activation being greater in comparison to the spread of activation in our study (Dieter et al. 2020). However, there are many key differences between Dieter et al.'s study and our study that should be noted, including species (gerbils versus mice), method of genetic modification (AAV versus transgenic), opsin (CatCh versus ChR2-H134R), and the size and pitch of LEDs (four 60 × 60 μm micro-LEDs versus one 270 × 220 μm micro-LED).

Spread of activation from an array of LEDs implanted in the human cochlea is likely to be quite different to the rodent studies described above due to the size differences. Accordingly, Keppeler et al. simulated the spread of light from the LEDs (250 × 200 μm, 473 nm) within a reconstructed non-human primate cochlea using X-ray phase-contrast tomography and light-sheet fluorescence microscopy (Keppeler et al. 2021). Keppeler et al.'s model predicted that the maximum spread of excitation would be approximately 1 octave, and the minimum spread would be 0.4 octaves. Another similar simulation with LEDs (653 nm) and laser-coupled waveguide by Khurana et al. in the 3D reconstructed human cochlea predicted the spectral spread using the full width at half maximum (FWHM). The median spectral spread observed during the optical stimulation with the LEDs was estimated to be 1.82 mm in the human cochlea (Khurana et al. 2022). In contrast, Jürgens et al. used electrical field imaging to estimate the current spread during electrical stimulation for cochlear implant users. The median spectral spread of excitation from 14 electrical cochlear implant users averaged across 22 channels was 8 mm, and for the best subject (CI user with least spread of excitation) was 4.13 mm at FWHM (Jürgens et al. 2018), suggesting a minimum 2-fold reduction in spread of activation could be achieved in humans using optical methods. In our study, we compared the spread of activation with a different parameter (d'=1 and 2 above the threshold) for both electrical and optical stimulation and found a 2.1-fold reduction of the spread of activation during optical stimulation compared to electrical stimulation at d'=1 above threshold, and a 1.9-fold reduction at d'=2 above threshold. We further compared the spread of activation via comparison to acoustic narrowband noise stimulation. Using this measure, the activation width during optogenetic stimulation was most similar to 0.125 octave narrowband noise at d'=1 and d'=2, while the activation width during electrical stimulation was comparable to 0.5 octave narrowband noise. This comparison method may be useful to compare the spread of activation via different stimulation modalities in future studies.

4.2. Channel interactions

The number of independent channels for cochlear implant users is reported to be around seven for individuals exhibiting the highest level of speech intelligibility, whereas for those with low levels of speech recognition proficiency, the number of independent channels was just four (Friesen et al. 2001). It is clear that an increase in the number of independent channels (achieved via reduced channel interactions) will be beneficial to cochlear implant recipients. Using a forward masking technique method commonly used in cochlear implant users (Throckmorton and Collins 1999), Agarwal et al. investigated the interaction between channels during infrared stimulation in albino guinea pigs and showed that the interactions were less compared to electrical stimulation (Agarwal et al. 2021). The study used two optical fibres inserted into the cochlea through cochleostomies directing light towards the spiral ganglion in the basal turn. We measured channel interactions via threshold shifts on the best recording site in the IC, as used by Middlebrooks and Snyder to assess a novel auditory nerve electrode (Middlebrooks and Snyder 2007) and by George et al. to measure channel interactions during electrical stimulation in cats (George et al. 2015a). Our results show that interactions between channels are significantly lower using optical stimulation compared to electrical stimulation. This is the first study to investigate the interaction between channels during optogenetic stimulation either with laser or μLEDs. While our study was performed in mice, modelling data also suggest that it is possible to distinguish between different channels at an inter-LED spacing (centre-to-centre) of 0.55 mm, and even with the relatively large Lambertian emitters in the marmoset cochlea (Keppeler et al. 2021). Furthermore, in a modelling study in the human cochlea, up to 64 independent channels were achieved using waveguides with a numerical aperture of 0.5 (Khurana et al. 2022).

4.3. Limitations

This study demonstrated the results using a transgenic mouse where all neurons were transfected with ChR2-H134R. However, in practical applications, when a virus is utilised for opsin expression, it will not be possible to achieve expression of opsins in all neurons. As a result, it is necessary to verify spatial precision and channel interactions in AAV-injected mice. Additional research will be necessary to establish the applicability of these findings to animals with chronic implantation and stimulation, as other variables such as fibrous tissue formation around the implanted array (Fallon et al. 2022) could impact the findings. Introducing an optical modality to the cochlear implant poses additional challenges to translation, including but not limited to the need to align the micro-LEDs towards the spiral ganglion neurons. In this study, alignment of the light towards the spiral ganglion was based on optical thresholds and was not routinely confirmed with imaging methods such as microCT.

The ChR2-H134R opsin used in this study has relatively slow kinetics and is unlikely to elicit a steady state response of more than 50 Hz in the auditory system (Thompson et al. 2020). Since the auditory system typically requires stimulation around 450-500 Hz, it will be important to

use an opsin with faster kinetics that matches the temporal processing of the auditory system. An example would be Chronos. Indeed, Keppeler et al. demonstrated high-rate stimulation of Chronos-expressing SGNs in gerbils, up to 500 Hz (Keppeler et al. 2018). Alternatively, an approach that combined electrical stimulation and optogenetic stimulation revealed that the high temporal resolution of electrical stimulation could be harnessed while still maintaining much of the spatial resolution afforded by the optical stimulation (Hart et al. 2020, Thompson et al. 2020).

5. Conclusion

In an optogenetic mouse model, the influence of optical stimuli delivered on one channel on the threshold of another channel was similar to pure tone stimulation. This contrasts with monopolar electrical stimulation commonly used in conventional cochlear implants. This suggests that optogenetic stimulation has the potential to increase the number of independent channels and deliver simultaneous stimulation, conveying more speech information to the implant recipient. Therefore, optogenetic stimulation has the potential to greatly enhance speech intelligibility and frequency discrimination in cochlear implant users.

CRediT authorship contribution statement

Ajmal A. Azees: Conceptualization, Methodology, Software, Writing – original draft, Visualization, Formal analysis, Investigation, Writing – review & editing. **Alex C. Thompson:** Conceptualization, Methodology, Software. **Ross Thomas:** Resources. **Jenny Zhou:** Resources. **Patrick Ruther:** Resources. **Andrew K. Wise:** Conceptualization, Writing – review & editing. **Elise A. Ajay:** Writing – review & editing. **David J. Garrett:** Writing – review & editing, Supervision. **Anita Quigley:** Writing – review & editing, Supervision. **James B. Fallon:** Conceptualization, Methodology, Software, Formal analysis, Writing – review & editing. **Rachael T. Richardson:** Conceptualization, Methodology, Writing – original draft, Visualization, Formal analysis, Investigation, Writing – review & editing, Supervision, Funding acquisition.

Declaration of Competing Interest

There are no conflicts of interest to declare.

Data availability

Data will be made available on request.

Acknowledgements

The research in this publication was supported with funding from the National Health and Medical Research Council (NHMRC) GNT#2002523. Ajmal A. Azees is supported by RMIT University and the Bionics Institute PhD scholarship. The Bionics Institute acknowledges the support they receive from the Victorian Government through its Operational Infrastructural Support Program.

Supplementary materials

Supplementary material associated with this article can be found, in the online version, at doi:10.1016/j.heares.2023.108911.

References

Agarwal, A., Tan, X., Xu, Y., Richter, C.P., 2021. Channel interaction during infrared light stimulation in the cochlea. Lasers Surg. Med. https://doi.org/10.1002/lsm.23360.

Ajay, E.A., Trang, E.P., Thompson, A.C., Wise, A.K., Grayden, D.B., Fallon, J.B., Richardson, R.T., 2023. Auditory nerve responses to combined optogenetic and electrical stimulation in chronically deaf mice. J. Neural Eng. 20 (2), 026035 https://doi.org/10.1088/1741-2552/acc75f.

Ayub, S., Gentet, L.J., Fiáth, R., Schwaerzle, M., Borel, M., David, F., Barthó, P., Ulbert, I., Paul, O., Ruther, P., 2017. Hybrid intracerebral probe with integrated bare LED chips for optogenetic studies. Biomed. Microdevices 19, 1–12. https://doi.org/10.1007/s10544-017-0190-3.

Bali, B., Gruber-Dujardin, E., Kusch, K., Rankovic, V., Moser, T., 2022. Analyzing efficacy, stability, and safety of AAV-mediated optogenetic hearing restoration in mice. Life Sci. Allian. 5 (8) https://doi.org/10.26508/lsa.202101338.

Bali, B., Lopez de la Morena, D., Mittring, A., Mager, T., Rankovic, V., Huet, A.T., Moser, T., 2021. Utility of red-light ultrafast optogenetic stimulation of the auditory pathway. EMBO Mol. Med. 13 (6), e13391. https://doi.org/10.15252/emmm.202013391.

Berenstein, C.K., Mens, L.H., Mulder, J.J., Vanpoucke, F.J., 2008. Current steering and current focusing in cochlear implants: comparison of monopolar, tripolar, and virtual channel electrode configurations. Ear Hear. 29 (2), 250–260.

Bierer, J.A., Litvak, L., 2016. Reducing channel interaction through cochlear implant programming may improve speech perception: current focusing and channel deactivation. Trends Hear. 20, 17. https://doi.org/10.1177/2331216516653389.

Black, R.C., Clark, G.M., Patrick, J.F., 1981. Current distribution measurements within the human cochlea. IEEE Trans. Biomed. Eng. 28 (10), 721–725. https://doi.org/10.1109/TBME.1981.324668.

Cayce, J.M., Friedman, R.M., Chen, G., Jansen, E.D., Mahadevan-Jansen, A., Roe, A.W., 2014. Infrared neural stimulation of primary visual cortex in non-human primates. Neuroimage 84, 181–190. https://doi.org/10.1016/j.neuroimage.2013.08.040.

Cederholm, J.M., Froud, K.E., Wong, A.C., Ko, M., Ryan, A.F., Housley, G.D., 2012. Differential actions of isoflurane and ketamine-based anaesthetics on cochlear function in the mouse. Hear. Res. 292 (1-2), 71–79. https://doi.org/10.1016/j.heares.2012.08.010.

Chernov, M., Roe, A.W., 2014. Infrared neural stimulation: a new stimulation tool for central nervous system applications. Neurophotonics 1 (1), 011011. https://doi.org/10.1117/1.NPh.1.1.011011.

Deisseroth, K., 2015. Optogenetics: 10 years of microbial opsins in neuroscience. Nat. Neurosci. 18 (9), 1213–1225. https://doi.org/10.1038/nn.4091.

Dieter, A., Duque-Afonso, C.J., Rankovic, V., Jeschke, M., Moser, T., 2019. Near physiological spectral selectivity of cochlear optogenetics. Nat. Commun. 10 (1), 1–10. https://doi.org/10.1038/s41467-019-09980-7.

Dieter, A., Klein, E., Keppeler, D., Jablonski, L., Harczos, T., Hoch, G., Rankovic, V., Paul, O., Jeschke, M., Ruther, P., Moser, T., 2020. µLED-based optical cochlear implants for spectrally selective activation of the auditory nerve. EMBO Mol. Med. 12 (8), e12387. https://doi.org/10.15252/emmm.202012387.

Fallon, J.B., Dueck, W., Trang, E.P., Smyth, D., Wise, A.K., 2022. Effects of chronic implantation and long-term stimulation of a cochlear implant in the partial hearing cat model. Hear. Res. 426, 108470.

Friesen, L.M., Shannon, R.V., Baskent, D., Wang, X., 2001. Speech recognition in noise as a function of the number of spectral channels: Comparison of acoustic hearing and cochlear implants. J. Acoust. Soc. Am. 110 (2), 1150–1163. https://doi.org/10.1121/1.1381538.

Frijns, J.H., Dekker, D.M., Briaire, J.J., 2011. Neural excitation patterns induced by phased-array stimulation in the implanted human cochlea. Acta Otolaryngol. 131 (4), 362–370. https://doi.org/10.3109/00016489.2010.541939.

Fu, Q.J., Nogaki, G., 2005. Noise susceptibility of cochlear implant users: the role of spectral resolution and smearing. J. Assoc. Res. Otolaryngol. 6 (1), 19–27. https://doi.org/10.1007/s10162-004-5024-3.

George, S.S., Shivdasani, M.N., Wise, A.K., Shepherd, R.K., Fallon, J.B., 2015a. Electrophysiological channel interactions using focused multipolar stimulation for cochlear implants. J. Neural Eng. 12 (6), 066005 https://doi.org/10.1088/1741-2560/12/6/066005.

George, S.S., Wise, A.K., Fallon, J.B., Shepherd, R.K., 2015b. Evaluation of focused multipolar stimulation for cochlear implants in long-term deafened cats. J. Neural Eng. 12 (3), 036003 https://doi.org/10.1088/1741-2560/12/3/036003.

George, S.S., Wise, A.K., Shivdasani, M.N., Shepherd, R.K., Fallon, J.B., 2014. Evaluation of focused multipolar stimulation for cochlear implants in acutely deafened cats. J. Neural Eng. 11 (6), 065003 https://doi.org/10.1088/1741-2560/11/6/065003.

Hart, W.L., Richardson, R.T., Kameneva, T., Thompson, A.C., Wise, A.K., Fallon, J.B., Stoddart, P.R., Needham, K., 2020. Combined optogenetic and electrical stimulation of auditory neurons increases effective stimulation frequency-an *in vitro* study. J. Neural Eng. 17 (1), 016069 https://doi.org/10.1088/1741-2552/ab6a68.

Hernandez, V.H., Gehrt, A., Reuter, K., Jing, Z., Jeschke, M., Schulz, A.M., Hoch, G., Bartels, M., Vogt, G., Garnham, C.W., 2014. Optogenetic stimulation of the auditory pathway. J. Clin. Invest. 124 (3), 1114–1129. https://doi.org/10.1172/JCI69050.

Huang, C.Y., Yang, H.M., Sher, Y.J., Lin, Y.H., Wu, J.L., 2005. Speech intelligibility of Mandarin-speaking deaf children with cochlear implants. Int. J. Pediatr. Otorhinolaryngol. 69 (4), 505–511.

Jürgens, T., Hohmann, V., Büchner, A., Nogueira, W., 2018. The effects of electrical field spatial spread and some cognitive factors on speech-in-noise performance of individual cochlear implant users—a computer model study. PLoS One 13 (4), e0193842. https://doi.org/10.1371/journal.pone.0193842.

Kalkman, R.K., Briaire, J.J., Frijns, J.H., 2015. Current focussing in cochlear implants: an analysis of neural recruitment in a computational model. Hear. Res. 322, 89–98. https://doi.org/10.1016/j.heares.2014.12.004.

Keiler, S., Richter, C.P., 2001. Cochlear dimensions obtained in hemicochleae of four different strains of mice: CBA/CaJ, 129/CD1, 129/SvEv and C57BL/6J. Hear. Res. 162 (1-2), 91–104. https://doi.org/10.1016/s0378-5955(01)00374-4.

Keppeler, D., Kampshoff, C.A., Thirumalai, A., Duque-Afonso, C.J., Schaeper, J.J., Quilitz, T., Töpperwien, M., Vogl, C., Hessler, R., Meyer, A., 2021. Multiscale photonic imaging of the native and implanted cochlea. Proc. Natl. Acad. Sci. 118 (18), e2014472118.

Keppeler, D., Merino, R.M., Lopez de la Morena, D., Bali, B., Huet, A.T., Gehrt, A., Wrobel, C., Subramanian, S., Dombrowski, T., Wolf, F., 2018. Ultrafast optogenetic stimulation of the auditory pathway by targeting-optimized Chronos. EMBO J. 37 (24), e99649. https://doi.org/10.15252/embj.201899649.

Keppeler, D., Schwaerzle, M., Harczos, T., Jablonski, L., Dieter, A., Wolf, B., Ayub, S., Vogl, C., Wrobel, C., Hoch, G., Abdellatif, K., Jeschke, M., Rankovic, V., Paul, O., Ruther, P., Moser, T., 2020. Multichannel optogenetic stimulation of the auditory pathway using microfabricated LED cochlear implants in rodents. Sci. Transl. Med. 12 (553) https://doi.org/10.1126/scitranslmed.abb8086.

Khurana, L., Keppeler, D., Jablonski, L., Moser, T., 2022. Model-based prediction of optogenetic sound encoding in the human cochlea by future optical cochlear implants. Comput. Struct. Biotechnol. J. 20, 3621–3629. https://doi.org/10.1016/j.csbj.2022.06.061.

Klein, E., Gossler, C., Paul, O., Ruther, P., 2018. High-density µLED-based optical cochlear implant with improved thermomechanical behavior. Front. Neurosci. 12, 659. https://doi.org/10.3389/fnins.2018.00659.

Klein, E., Kaku, Y., Paul, O., Ruther, P., 2019. Flexible µled-based optogenetic tool with integrated µ-lens array and conical concentrators providing light extraction improvements above 80%. In: Proceedings of the 2019 IEEE 32nd International Conference on Micro Electro Mechanical Systems (MEMS). IEEE.

Landry, T.G., Fallon, J.B., Wise, A.K., Shepherd, R.K., 2013. Chronic neurotrophin delivery promotes ectopic neurite growth from the spiral ganglion of deafened cochleae without compromising the spatial selectivity ofcochlear implants. J. Comp. Neurol. 521 (12), 2818–2832. https://doi.org/10.1002/cne.23318.

Landsberger, D.M., Srinivasan, A.G., 2009. Virtual channel discrimination is improved by current focusing in cochlear implant recipients. Hear. Res. 254 (1-2), 34–41. https://doi.org/10.1016/j.heares.2009.04.007.

Litvak, L.M., Spahr, A.J., Emadi, G., 2007. Loudness growth observed under partially tripolar stimulation: model and data from cochlear implant listeners. J. Acoust. Soc. Am. 122 (2), 967–981. https://doi.org/10.1121/1.2749414.

Middlebrooks, J.C., Snyder, R.L., 2007. Auditory prosthesis with a penetrating nerve array. J. Assoc. Res. Otolaryngol. 8, 258–279.

Ou, H.C., Bohne, B.A., Harding, G.W., 2000a. Noise damage in the C57BL/CBA mouse cochlea. Hear. Res. 145 (1-2), 111–122. DOI: S0378-5955(00)00081-2 [pii].

Ou, H.C., Harding, G.W., Bohne, B.A., 2000b. An anatomically based frequency–place map for the mouse cochlea. Hear. Res. 145 (1-2), 123–129.

Peterson, E., Tyler, D., 2013. Motor neuron activation in peripheral nerves using infrared neural stimulation. J. Neural Eng. 11 (1), 016001 https://doi.org/10.1088/1741-2560/11/1/016001.

Pfingst, B.E., Xu, L., 2004. Across-site variation in detection thresholds and maximum comfortable loudness levels for cochlear implants. J. Assoc. Res. Otolaryngol. 5 (1), 11–24. https://doi.org/10.1007/s10162-003-3051-0.

Poursoroush, S., Ghorbani, A., Soleymani, Z., Kamali, M., Yousefi, N., Poursoroush, Z., 2015. Speech Intelligibility of Cochlear-Implanted and Normal-Hearing Children. Iran. J. Otorhinolaryngol. 27 (82), 361.

Rebscher, S.J., Snyder, R.L., Leake, P.A., 2001. The effect of electrode configuration and duration of deafness on threshold and selectivity of responses to intracochlear electrical stimulation. J. Acoust. Soc. Am. 109 (5), 2035–2048. https://doi.org/10.1121/1.1365115.

Richardson, R.T., Ibbotson, M.R., Thompson, A.C., Wise, A.K., Fallon, J.B., 2020. Optical stimulation of neural tissue. Healthc. Technol. Lett. 7 (3), 58–65. https://doi.org/10.1049/htl.2019.0114.

Richardson, R.T., Thompson, A.C., Wise, A.K., Ajay, E.A., Gunewardene, N., O'Leary, S. J., Stoddart, P.R., Fallon, J.B., 2021. Viral-mediated transduction of auditory neurons with opsins for optical and hybrid activation. Sci. Rep. 11 (1), 1–17. https://doi.org/10.1038/s41598-021-90764-9.

Richter, C.P., Rajguru, S., Matic, A., Moreno, E., Fishman, A., Robinson, A., Suh, E., Walsh, J., 2011. Spread of cochlear excitation during stimulation with pulsed infrared radiation: inferior colliculus measurements. J. Neural Eng. 8 (5), 056006 https://doi.org/10.1088/1741-2560/8/5/056006.

Snyder, R.L., Bierer, J.A., Middlebrooks, J.C., 2004. Topographic spread of inferior colliculus activation in response to acoustic and intracochlear electric stimulation. J. Assoc. Res. Otolaryngol. 5 (3), 305–322. https://doi.org/10.1007/s10162-004-4026-5.

Thompson, C., Stoddart, A.P.R., Jansen, E.D., 2014. Optical stimulation of neurons. Curr. Mol. Imaging (Discontin.) 3 (2), 162–177. https://doi.org/10.2174/2211555203666141117220611.

Thompson, A., Wise, A.K., Hart, W., Needham, K., Fallon, J.B., Gunewardene, N., Stoddart, P.R., Richardson, R.T., 2020. Hybrid optogenetic and electrical stimulation for greater spatial resolution and temporal fidelity of cochlear activation. J. Neural Eng. 17 (5) https://doi.org/10.1088/1741-2552/abbff0.

Throckmorton, C.S., Collins, L.M., 1999. Investigation of the effects of temporal and spatial interactions on speech-recognition skills in cochlear-implant subjects. J. Acoust. Soc. Am. 105 (2), 861–873. https://doi.org/10.1121/1.426275.

Wells, J.D., Kao, C., Jansen, E.D., Konrad, P.E., Mahadevan-Jansen, A., 2005. Application of infrared light for *in vivo* neural stimulation. J. Biomed. Opt. 10 (6), 064003 https://doi.org/10.1117/1.2121772.

Wilson, B.S., Dorman, M.F., 2008. Cochlear implants: a remarkable past and a brilliant future. Hear. Res. 242 (1-2), 3–21. https://doi.org/10.1016/j.heares.2008.06.005.

Wolf, B.J., Kusch, K., Hunniford, V., Vona, B., Kühler, R., Keppeler, D., Strenzke, N., Moser, T., 2022. Is there an unmet medical need for improved hearing restoration? EMBO Mol. Med. 14 (8), e15798.

Wrobel, C., Dieter, A., Huet, A., Keppeler, D., Duque-Afonso, C.J., Vogl, C., Hoch, G., Jeschke, M., Moser, T., 2018. Optogenetic stimulation of cochlear neurons activates the auditory pathway and restores auditory-driven behavior in deaf adult gerbils. Sci. Transl. Med. 10 (449) https://doi.org/10.1126/scitranslmed.aao0540.

Zgierski-Johnston, C.M., Ayub, S., Fernández, M., Rog-Zielinska, E., Barz, F., Paul, O., Kohl, P., Ruther, P., 2020. Cardiac pacing using transmural multi-LED probes in channelrhodopsin-expressing mouse hearts. Prog. Biophys. Mol. Biol. 154, 51–61. https://doi.org/10.1016/j.pbiomolbio.2019.11.004.